

## Materials Science | Hot Paper |

## Sponge-Like Behaviour in Isorecticular Cu(Gly-His-X) Peptide-Based Porous Materials

Carlos Martí-Gastaldo,<sup>\*[a, c]</sup> John E. Warren,<sup>[a, d]</sup> Michael E. Briggs,<sup>[a]</sup> Jayne A. Armstrong,<sup>[b]</sup> K. Mark Thomas,<sup>[b]</sup> and Matthew J. Rosseinsky<sup>\*[a]</sup>

**Abstract:** We report two isorecticular 3D peptide-based porous frameworks formed by coordination of the tripeptides Gly-L-His-Gly and Gly-L-His-L-Lys to Cu<sup>II</sup> which display sponge-like behaviour. These porous materials undergo structural collapse upon evacuation that can be reversed by exposure to water vapour, which permits recovery of the original open channel structure. This is further confirmed by sorption studies that reveal that both solids exhibit selective

sorption of H<sub>2</sub>O while CO<sub>2</sub> adsorption does not result in recovery of the original structures. We also show how the pendant aliphatic amine chains, present in the framework from the introduction of the lysine amino acid in the peptidic backbone, can be post-synthetically modified to produce urea-functionalised networks by following methodologies typically used for metal-organic frameworks built from more rigid "classical" linkers.

## Introduction

Metal-organic frameworks (MOFs) or porous coordination polymers (PCPs) are crystalline micro- or nanoporous materials built from the interconnection of metal ions or clusters and organic linkers.<sup>[1]</sup> It is their extraordinary synthetic and structural versatility, together with the predictability of the targeted frameworks that account for the remarkable growth that the synthesis and study of this type of materials has experienced. Once evacuated, these frameworks often present high porosity and internal surface areas that can be used for a plethora of applications like gas storage<sup>[2]</sup> and/or separation,<sup>[3]</sup> heterogene-

ous catalysis,<sup>[4]</sup> sensing<sup>[5]</sup> or proton conduction<sup>[6]</sup> amongst others.

Framed in this general context, particular interest has lately been devoted to the development of isorecticular homochiral MOFs by the incorporation of enantiomerically pure linkers in their backbone.<sup>[7]</sup> The interest in these materials resides in their use as asymmetric catalysts and chiral adsorbents that can benefit from the enantioselective recognition that originates from the different host-guest intermolecular interactions for a given enantiomer.

Besides chirality, the introduction of guest-accessible functional organic sites (FOS) also represents a valid route to modify the functional behaviour of MOFs.<sup>[8]</sup> These chemical groups are borne by the organic linker, reside in the internal surface of the pore after the formation of the framework and can modify its chemical nature and therefore its affinity for specific guests with important implications in their catalytic activity and selective sorption. Despite these promising features, examples describing the combination of chirality and FOS in a single MOF remain very scarce. This is likely due to the insufficient library of candidates. Whereas the number of enantiopure ligands available is already limited per se, if they have to be chemically engineered to incorporate functional groups that will not coordinate the metal nodes and will remain free in the pores of the host, the number is reduced even further.

In this context, the use of naturally occurring oligopeptides is worthy of exploration as they represent a rich source of chiral linkers that can incorporate a wide variety of FOS determined by the choice of amino acids (aa's). In contrast to the use of other biologically derived molecules like simple aa's<sup>[9]</sup> or nucleobases<sup>[10]</sup> that has already proved fruitful, the design of peptide-based open frameworks is still in its infancy.<sup>[11]</sup> We recently reported how the reaction of Zn<sup>II</sup> ions with dipeptides like carnosine ( $\beta$ -alanyl-L-histidine) yields ZnCar, a ZIF-type 3D

[a] Dr. C. Martí-Gastaldo, Dr. J. E. Warren, Dr. M. E. Briggs, Prof. M. J. Rosseinsky

Department of Chemistry, University of Liverpool  
Crown Street, Liverpool, L69 7ZD (UK)  
E-mail: m.j.rosseinsky@liverpool.ac.uk

[b] Dr. J. A. Armstrong, Prof. K. M. Thomas

Wolfson Northern Carbon Reduction Laboratories, School of Chemical Engineering and Advanced Materials, Newcastle University  
Newcastle upon Tyne, NE1 7RU (UK)

[c] Dr. C. Martí-Gastaldo

Instituto de Ciencia Molecular (ICMol), Universidad de Valencia  
Paterna, 46980 (Spain)  
E-mail: carlos.marti@uv.es

[d] Dr. J. E. Warren

School of Materials, The University of Manchester  
Sackville Street, Manchester, M1 3BB (UK)

Supporting information for this article is available on the WWW under <http://dx.doi.org/10.1002/chem.201502098>.

© 2015 The Authors. Published by Wiley-VCH Verlag GmbH & Co. KGaA. This is an open access article under the terms of the Creative Commons Attribution Non-Commercial NoDerivs License, which permits use and distribution in any medium, provided the original work is properly cited, the use is non-commercial and no modifications or adaptations are made.

water-stable MOF,<sup>[12]</sup> whereas introduction of Gly-Ala, Gly-Ser and Gly-Thr direct the formation of layered porous materials, Zn(Gly-X)<sub>2</sub>, that exhibit adaptable porosity after disordered (X=Ala)<sup>[13]</sup> or ordered (X=Ser) closure<sup>[14]</sup> of the framework after guest removal or classical sorption response (X=Thr).<sup>[15]</sup> This distinct behaviour is controlled in all cases by the conformational flexibility, chemistry of the aa's sidechain and their sequence in the peptidic backbone. Still, the internal surface area accessible in these biomimetic materials remains comparatively small therefore limiting the size of the guests that can be loaded and the functionalities accessible within these chiral, chemically functionalised pores.

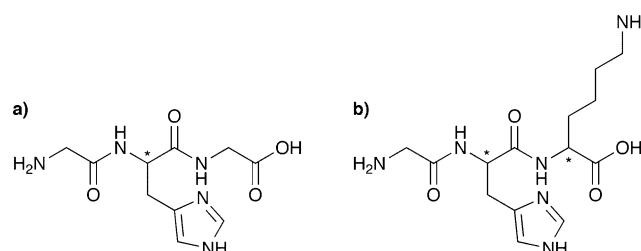
We demonstrate how the use of longer tripeptides permits increasing the pore metrics in isorecticular peptide-based open frameworks with three-dimensional pores whilst leading to increased flexibility, as enabled by the wider conformational range accessible to the linker. Here, this structural flexibility is complemented with the introduction of FOS in the pores thus leading to sponge-like behaviour in the presence of water. In addition, we show how these FOS can be used as a versatile platform to modify the chemical nature of these biomimetic frameworks by post-synthetic modification (PSM).

## Results and Discussion

### Synthesis and structure

Reaction of the peptides glycyl-L-histidylglycine and glycyl-L-histidyl-L-lysine (Scheme 1) with copper(II) acetate in an ethanolic solution led to the formation of [Cu(GHG)]·(H<sub>2</sub>O)<sub>10</sub>(EtOH)<sub>1</sub> (**1**; GHG = C<sub>12</sub>H<sub>16</sub>N<sub>6</sub>O<sub>5</sub><sup>2-</sup>) and [Cu(GHK)]·(H<sub>2</sub>O)<sub>5.5</sub> (**2**; GHK = C<sub>14</sub>H<sub>22</sub>N<sub>6</sub>O<sub>4</sub><sup>2-</sup>), respectively. They can be isolated as deep-blue prismatic crystals by controlled layering of ethanol onto an aqueous solution containing the metal and the linker in a 1:1 ratio (see the Experimental Section). Both structures have previously been reported CSD reference codes **1**: GLHGCU (1169243), GHSVCU (1167185), GHGCU (1167181) (perchlorate

salt)<sup>[16]</sup> and **2**: OZEBIF (809108), CIDNIM (1124899).<sup>[17]</sup> However we report here a novel form for **1** and a redetermination for **2**. Unlike other authors, we focus on the 3D extended structure and associated void space of these unconventional porous materials.



**Scheme 1.** Tripeptides: a) glycyl-L-histidylglycine (GHG), and b) glycyl-L-histidyl-L-lysine (GHK). Stars represent chiral centres.

Compounds **1** and **2** crystallise in the enantiomorphic tetragonal space group *P*4<sub>1</sub>2<sub>1</sub>2, compared with GLHGCU that was reported in the monoclinic *C*<sub>2</sub> space group. Homochirality is confirmed by the Flack and Hooft parameter values that are 0.019(11) and 0.03(2), and 0.033(5) and 0.064(4), for **1** and **2**, respectively.<sup>[18]</sup> In these isorecticular frameworks, each Cu<sup>II</sup> centre adopts a distorted square-based pyramidal configuration. The terminal amino group (N10) and the imine nitrogen atom (N7) belonging to the terminal Gly together with the histidine nitrogen atom (N3) belonging to the His residue form a tridentate chelate that occupies three basal positions. This binding mode is rather specific to the complexation of copper with peptides containing a histidyl residue which is known to be an important metal-binding site in proteins.<sup>[19]</sup> It is also isostructural with the previous reported determinations. The coordination sphere is completed by two monodentate carboxylate groups belonging to either the terminal Gly or Lys residues, in **1** and **2**, respectively, that occupy the apical and the remaining basal position (Figure 1 a). The formation of the chelate leads to N–

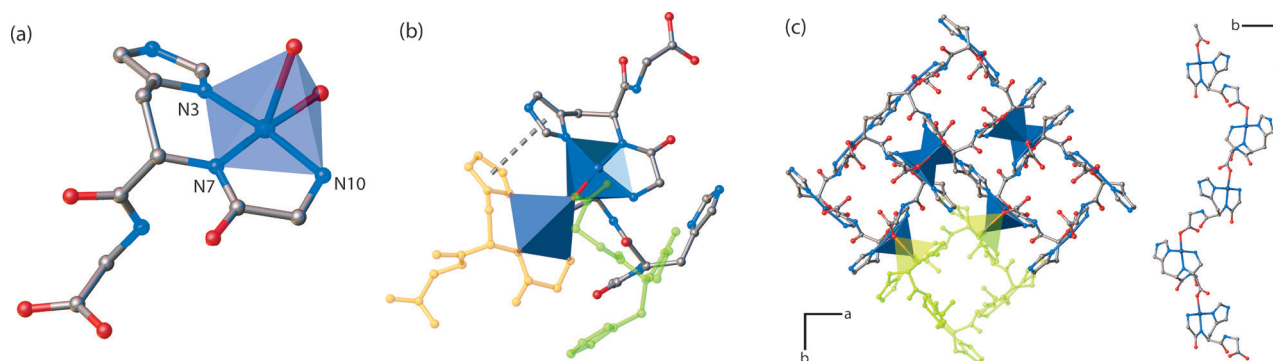


**Figure 1.** Structure of as-made Cu(GHG) and Cu(GHK) frameworks. a) Square planar pyramidal geometry of the Cu<sup>II</sup> metal centre. b) Perspective of the binuclear cluster that acts as secondary building unit. The two different types of peptide-to-metal interaction are highlighted: tridentate chelate with the His-X residue (orange) and monodentate carboxylate bond with the C-terminal Gly (green). The dashed line stands for the  $\pi$ -interaction between neighbouring histidine side-chains that contribute to the stabilization and formation of the dimer. c) Perspective showing how the sequence Cu-peptide-Cu defines fourfold helical chains (right) that are bridged into a three-dimensional framework by the formation of  $\mu_2$ -carboxylate bridges. Although the pictures correspond to the Cu(GHG) framework these structural details also apply to Cu(GHK). Hydrogen atoms have been omitted for clarity. Cu, dark blue; O, red; C, grey; N, blue; H, white.

Cu distances varying between 1.952(2)–2.005(2) for **1** and 1.952(3)–2.006(3) Å for **2**. As for the coordination of the carboxylate groups, the O1–Cu1 distances are substantially longer for the apical, 2.4739(17) and 2.516(2), than for the basal positions ranging from 1.991(2) to 1.977(2) Å, for **1** and **2**, respectively.

These carboxylate groups also act as  $\mu_2$ -bridging ligands and link two neighbouring metal centres to form a dimer composed of two inverted square pyramids sharing edges (Figure 1b). Formation of this binuclear cluster is additionally reinforced by the presence of supramolecular  $\pi$ -interactions between neighbouring imidazole rings belonging to two tripeptide molecules that exhibit a parallel-displaced stacking with a centroid-to-centroid distance of 3.635 and 3.585 Å for **1** and **2**, respectively. This is consistent with previous studies that confirm this orientation to be more favourable energetically for the interaction of aromatic side chains in proteins,<sup>[20]</sup> and highlight the pivotal role played by non-covalent interactions in controlling the dimensionality of peptide-based frameworks. It is also noteworthy that in both structures there are water molecules located in the remaining apical positions but at significantly longer distances of 3.307(2) and 3.183(6) Å. The recurrence of this position can be attributed to either large Jahn–Teller distortions or more likely to a hydrogen bonding interaction to the Gly or Lys amide nitrogen (N17).

As result of the metal binding the peptidic linkers show specific conformations,  $\Phi$ ,  $\Psi$  and  $\omega$ , which are defined by the torsion parameters of their constituent amino acids. These values are summarized in Table 1 and Table S8 in the Supporting Information. The use of tripeptides introduces a higher degree of conformational flexibility of the connectors with respect to the use of dipeptides that are restricted to two torsional coordinates,  $\Phi$  and  $\Psi$ .<sup>[13–15]</sup> This increased flexibility has an important impact on the structural stability of **1** and **2** (vide infra).

**Table 1.** Torsion angles for the Gly-L-His-Gly and Gly-L-His-L-Lys tripeptides in **1** and **2**, respectively.

Compounds	$\Phi$ [°] N-term Gly	$\Psi$ [°] His	$\omega$ [°] C-term Gly
<b>1</b>	130.8(2)	–178.7(2)	5.6(3)
<b>2</b>	130.3(4)	–173.7(3)	2.8(5)

It is worthwhile highlighting the role played by the  $\mu_2$ -carboxylate bridge in controlling the dimensionality of these materials in the solid state as it interconnects the neighbouring fourfold helicoidal chains, which result from the interaction of one peptide with two Cu<sup>II</sup> centres via the C-terminal residue and the N-terminal Gly and His amino acids, into a three dimensional array (Figure 1c). As a result, **1** and **2** display an open 3D channel structure that is occupied by water and ethanol molecules in **1** and water and the Lys chain in **2** in the as-made solids. On the contrary, previous examples describe how the substitution of the  $\mu_2$ -monodentate carboxylate bridge with water molecules provokes a reduction of the dimensionality to produce 1D chains interconnected via H bonds, with the subsequent loss of intrinsic porosity.<sup>[21,34]</sup>

Removal of the guest molecules gives access to a 3D open structure in both materials which is a product of the interconnection of 1D pores (Figure 2). According to the structural analysis,<sup>[22]</sup> these provide a solvent-accessible volume of 60.2 and 47.2 [48.5] % of the total volume of **1** and **2** (disordered components A[B]), respectively (3232.2 and 2642.4 [2711.0] Å<sup>3</sup> per unit cell at 100 K; see Table S9 in the Supporting Information for further details). Comparing the loaded and simulated desolvated structures allows for an estimate of the volume occupied by the guests per unit cell. The calculated molecular volume occupied by the guest being 30.45 and 17.17 [15.73] % for **1** and **2**, respectively, with the aliphatic Lys chain occupying approximately 50% of the available space. Hence, the use of tripeptides as linkers leads to substantially higher intrinsic porosities in comparison with the use of dipeptides that reach a maximum value of 28% in [Zn(Gly-Ala)<sub>2</sub>].<sup>[13]</sup>

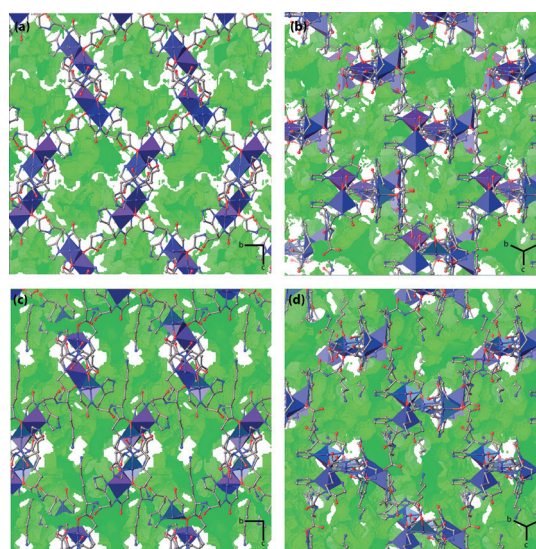


**Figure 2.** View of the three-dimensional porosity in Cu(GHG) (top) and Cu(GHK) (bottom). Surface representation of the 3D porosity (pale green, probe radius 1.2 Å) that results from the interconnection of 1D pores in the open structure of **1** (top) and **2** (bottom). Perspective along [100] (a and c) and [111] (b and d) directions showing the presence 3D channels decorated by a variety of FOS from the peptidic backbone. Hydrogen atoms have been omitted for clarity.

Due to the lattice type a view along the directions [100] and [010] reveals the presence of one three-dimensional channel in the desolvated solids (Figure 2). Sampling of the void space with a spherical probe of 1.2 Å by using Voronoi decomposition<sup>[23]</sup> affords largest included spheres ( $D_i$ ) and largest free spheres ( $D_f$ ) with diameters of 23.4 and 22.0 [21.9] Å ( $D_i$ ) and 21.0 and 19.0 [19.1] Å ( $D_f$ ) for **1** and **2**. The surface of these channels is decorated with imidazole, amino, amide and carboxylate groups from the peptidic backbone. These are oriented towards the centres of the pores, hence modifying their chemical nature and polarity, and will act as FOS by controlling the interaction between the host and the loaded guests. Substitution of glycine (Gly) with the lysine (Lys) aa in the C-terminal residue in **2** introduces an aliphatic amine moiety in the cavities. This amino group can act as a hydrogen bond donor/

acceptor and has been generally used as a base in catalysis.<sup>[24]</sup> In addition, this FOS can be further subjected to PSM therefore introducing an additional tool for chemical modification of the surface of the channels.

According to the refined structural models at 100 K, ten molecules of water and one molecule of EtOH occupy the open channel structure in **1** whilst the presence of aliphatic amines in the pores of **2** lead to a reduced solvent content with 5.5 disordered molecules of water per formula unit. CHN data reflect the presence of a smaller amount of solvent molecules in the analysed crystals with only 6 and 5 water molecules being present in **1** and **2**, respectively. This deviation suggests that the solvent is partially removed by evaporation under room temperature conditions. This is consistent with our thermogravimetric studies that provide almost identical solvent content for freshly prepared materials (Figure S11 in the Supporting Information).

The solids are insoluble in methanol or ethanol and common organic solvents but are readily dissolved when suspended in water. Phase purity was confirmed with PXRD (Figure 3: GHGa and GHKa). Refinement of the powder patterns with the unit cell calculated from the atomic positional parameters of the single-crystal data discards the presence of contaminant phases (Figures S12–S18 in the Supporting Information). Overnight evacuation of the solids at room temperature under dynamic vacuum ( $10^{-6}$  mbar) triggers a structural collapse of the frameworks that exhibit amorphous PXRD patterns (Figure 3: GHGb and GHKb). This crystalline-to-amorphous transformation is connected to the desolvation of the

frameworks as confirmed by the CHN analyses of the materials after evacuation. This scenario is indicative of the high flexibility of the frameworks associated with the introduction of tripeptides as intermetallic connectors, which provide a wider range of accessible conformations. We have recently described how the torsional response of peptidic struts in response to environmental changes can be controlled by their sidechain. Whereas Gly-Thr remains conformationally invariant in Zn(Gly-Thr)<sub>2</sub>,<sup>[15]</sup> Zn(Gly-Ser)<sub>2</sub> displays conformationally ordered closure into a desolvated crystalline state upon guest removal.<sup>[14]</sup> To correlate this amorphisation with the microstructure of the solids we studied the effects of evacuation on the morphology of as-made and desolvated crystals. SEM examination reveals that evacuation introduces multiple cracks across the facets of the desolvated crystals probably originating from the mechanical strain associated with the removal of the guest molecules filling the nanopores (Figures S19 and S20 in the Supporting Information).<sup>[25]</sup>

Next, the amorphous desolvated solids were transferred to a vial and exposed over 72 h to the vapours of H<sub>2</sub>O, a 50:50% (v/v) mixture of H<sub>2</sub>O and EtOH, EtOH and MeOH (c, d, e and f in Figure 3). Whilst exposure to EtOH or MeOH does not affect the amorphous state, the presence of water triggers a structural transformation as both materials recover their original structures. It is worthwhile mentioning that similar sponge-like behaviour—that is reversible amorphous-to-crystalline structural transformation upon re-solution, also called Type-I “recoverable collapsing”—has been described for other dynamic coordination polymers.<sup>[8,25–28]</sup>

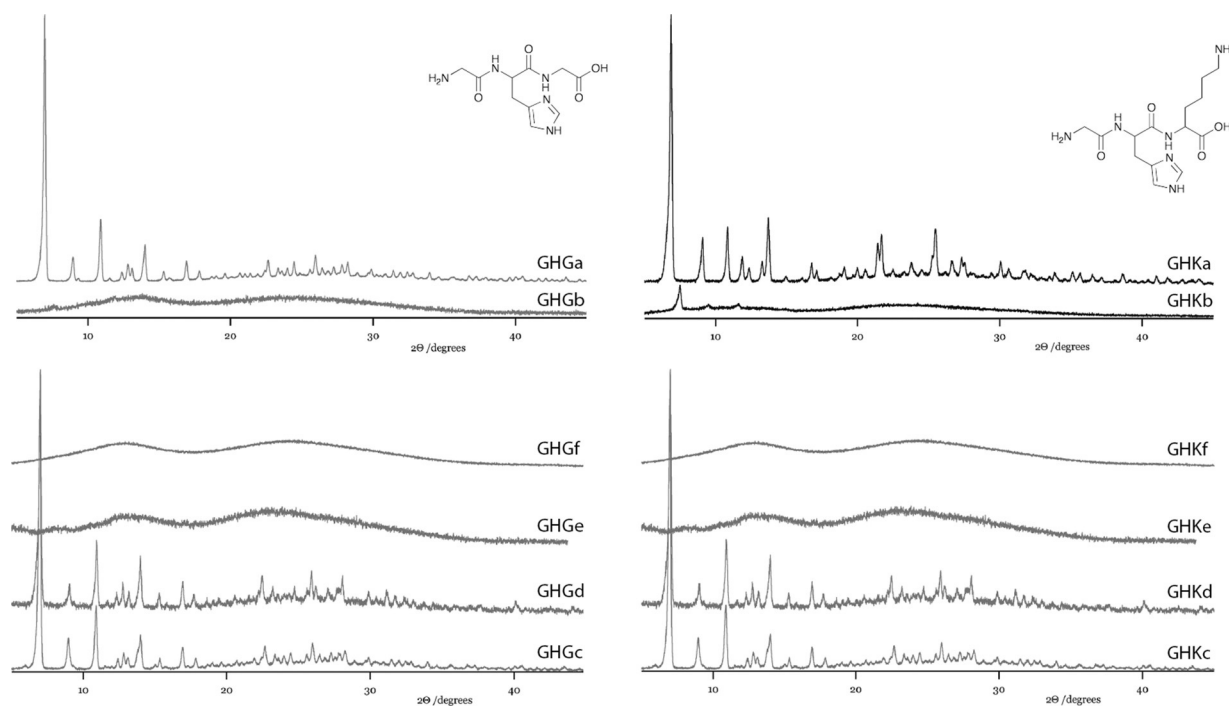


**Figure 3.** Sponge-like amorphous-to-crystalline structural transformation of Cu(GHG) (left) and Cu(GHK) (right). PXRD patterns of the as-made (a) and desolvated (b) Cu(GHG) (**1**) and Cu(GHK) (**2**) (top). PXRD of the solids after exposing the amorphous desolvated structure to the vapours of H<sub>2</sub>O (c), 50:50% (v/v) mixture of H<sub>2</sub>O and EtOH (d), EtOH (e) and MeOH (f). See Figures S12–18 in the Supporting Information for the refined unit cell parameters corresponding to the crystalline powder and their comparison with unit cell parameters extracted from single-crystal structures.

## Adsorption studies

The formation of intrinsic porosity in the solids was studied gravimetrically for CO<sub>2</sub> and H<sub>2</sub>O adsorption in an intelligent gravimetric analyser (IGA). Freshly prepared samples of **1** (GHG) and **2** (GHK) were evacuated and heated at 80 °C under ultrahigh vacuum until degassing was complete. Complete desolvation was confirmed from the observed desorption profile. The weight losses, for the multiple batches studied, were in agreement with the solvent content extracted from the CHN and TGA analyses (vide supra). The frameworks only exhibited very low CO<sub>2</sub> uptakes at 195 and 298 K at 1 and 10 bar, respectively (Figure S21 in the Supporting Information). This confirms that structural collapse occurs during desolvation closing the channels of the framework so that they are not accessible for CO<sub>2</sub> under the above conditions.

Since the open channel structure can be recovered in the presence of water, the H<sub>2</sub>O sorption experiments were investigated. The reproducibility of the measurements was confirmed for independent batches and several sorption cycles. Figure 4a and b show the water vapour adsorption isotherms of the solids **1** and **2** at 299–307 K. The main differences in isotherm shape are at uptakes > 11 mmol g<sup>-1</sup>. The isotherms are consistent with low availability of hydrophilic sites for water sorption in the amorphous state with uptake gradually increasing as the crystalline structure is formed. This indicates that the amorphous state has a predominantly hydrophobic accessible surface. The isotherms involve structural switching in soft porous

materials and result from the amorphous/closed-to-crystalline/open structural rearrangement. At high loading, the adsorption interaction is mainly associated with the H-bond interaction between adsorbed water molecules whereas, at low loading, framework structure and interaction with surface sites are involved. The uptake values at 299 K and pressure of 31 mbar ( $p/p^0=0.92$ ), were 20.85 and 18.08 mmol g<sup>-1</sup> for **1** and **2**, respectively. These uptakes correspond to loadings of 8.1 (0.376 g g<sup>-1</sup>) and 7.3 (0.326 g g<sup>-1</sup>) molecules of water per unit formula for **1** and **2**, respectively. These values are close to the solvent content extracted from the structural analysis on as-made crystals of both materials.

Although the water vapour adsorption isotherms were hysteretic and the structure was developing during the adsorption process, the graphs of ln(*P*) versus the reciprocal of temperature were linear for the isotherms. The apparent isosteric enthalpy of adsorption (*Q*<sub>st</sub>) and entropy of adsorption (Δ*S*) as a function of loading for water vapour sorption on **1** and **2** were determined by linear regression between adjacent isotherm points for adsorption isotherms and are shown in Figure 4c and d, respectively. It is apparent that at low-pressures, the sorption of water vapour on **2** is lower than **1** in the range used for *Q*<sub>st</sub> calculations. The isosteric enthalpy at zero surface coverage is a fundamental measure of the H<sub>2</sub>O interaction with the framework. It is evident that the interaction of H<sub>2</sub>O with **1** (GHG) is significantly stronger than with **2** (GHK). The *Q*<sub>st</sub> for H<sub>2</sub>O adsorption on **1** decreases with increasing uptake while the values for **2** were lower (Figure 4c and d). The major

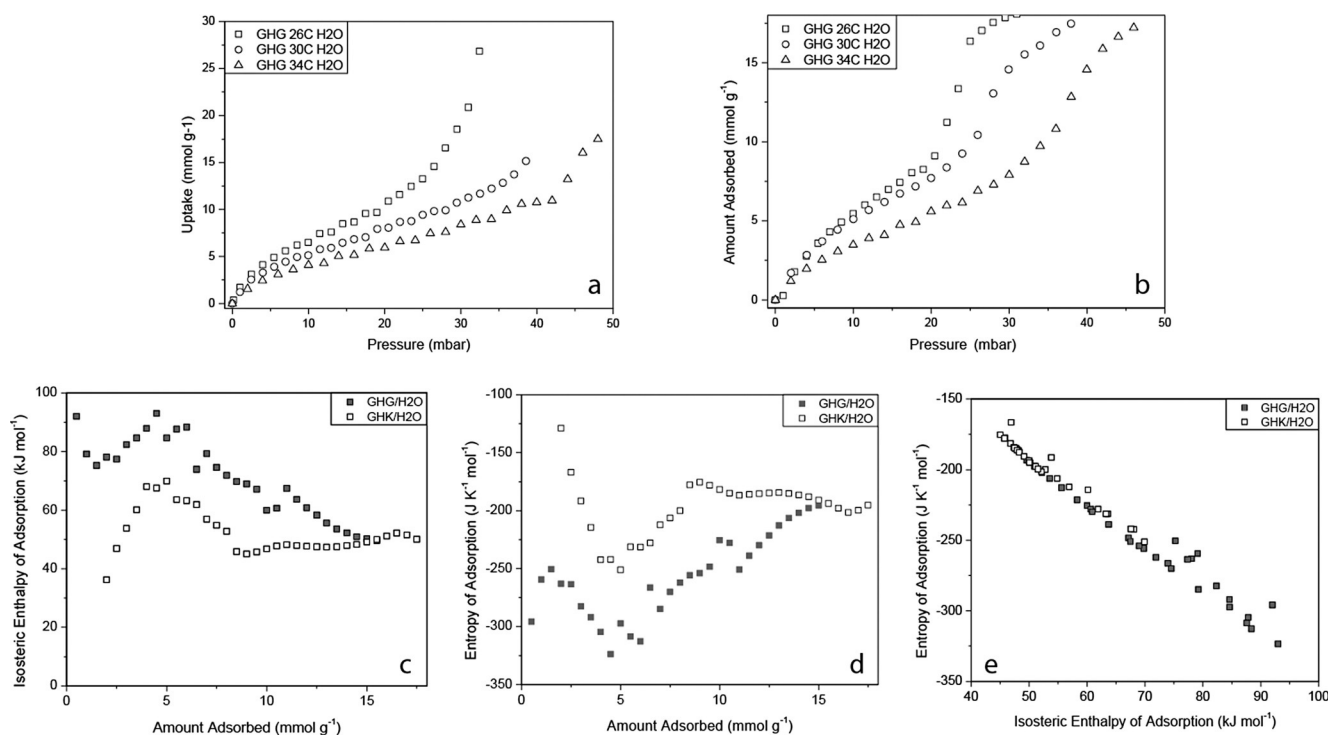
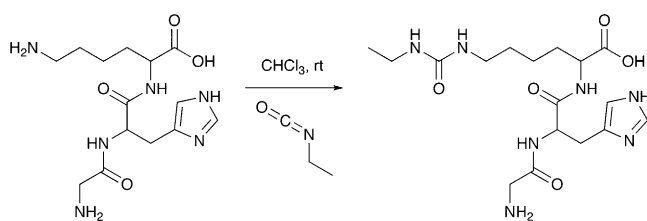


**Figure 4.** Water sorption of Cu(GHG) and Cu(GHK). a, b) H<sub>2</sub>O vapour sorption isotherms for **1** (GHG; a) and **2** (GHK; b); temperature range 26–34 °C. c, d) Variation of apparent isosteric enthalpy of adsorption (c) and entropy of adsorption (d) with the amount of water vapour sorption on **1** and **2** between 26 and 34 °C. The adsorption data for **2** include 20 and 38 °C isotherm data up to 6–7 mmol g<sup>-1</sup>. e) Variation of entropy of adsorption with isosteric enthalpy of adsorption for water vapour adsorption on **1** and **2**.

difference occurs where the collapsed amorphous frameworks are reforming the crystalline structure. This is attributed to the presence of Lys in the peptide linker in **2** since this is the only difference between the isorecticular frameworks. The introduction of the aliphatic amine side-chains within the pores influences intra-framework H bonds in **2** leading to difference in the energetics of structural change. At high uptakes the  $Q_{st}$  values for both **1** and **2** are slightly higher than the enthalpy of vaporization for H<sub>2</sub>O (43.99 kJ mol<sup>-1</sup> at 25 °C).<sup>[29]</sup> There is a correlation between the  $\Delta S$  and  $Q_{st}$  values for H<sub>2</sub>O adsorption on **1** and **2** (Figure 4e). It is evident that the enthalpy of adsorption is the driving force for structural change from amorphous to crystalline forms of **1** and **2**.

### Post-synthetic modification of Cu(Gly-His-Lys)

The presence of the Lys side-chain offers the potential for post-synthetic modification of framework **2**. This approach is commonly exploited for more rigid “classic” MOFs<sup>[30]</sup> but still remains unexplored for peptide-based porous materials. As-made crystals of **2** were solvent-exchanged in CHCl<sub>3</sub> and then treated with ethyl isocyanate by following a protocol previously described for the PSM of IRMOF-3 (Scheme 2).<sup>[31]</sup>



**Scheme 2.** Post-synthetic modification of the GHK tripeptide in **2** to introduce urea groups in the lysine side-chain by treatment with ethyl isocyanate.

After filtration, the crystals were thoroughly washed with CHCl<sub>3</sub> to remove the residual non-reacted isocyanate. FT-IR provided the first proof of the derivatization of the peptide in **2**<sub>PSM</sub> as it shows the presence of the characteristic urea C=O and N–C–N stretching vibrational modes at 1730 and 1307 cm<sup>-1</sup>, respectively (Figure S25 in the Supporting Information). This is additionally supported by <sup>1</sup>H NMR analysis of two independent batches that provide conversion yields close to 80% (Figures S3 and S4 in the Supporting Information). This is in good agreement with the conversion values of about 70% reported for the PSM of IRMOF-3 under equivalent synthetic conditions. As illustrated in Figure 5, the PXRD of **2**<sub>PSM</sub> confirms that the modification of the aliphatic amine takes place without significant loss of crystallinity as the material retains the original open structure of **2**.

### Conclusion

The combination of the tripeptides GHG and GHK with Cu<sup>II</sup> ions leads to the formation of two isorecticular 3D porous materials with higher solvent-accessible volumes (60.2 and 47.2%)

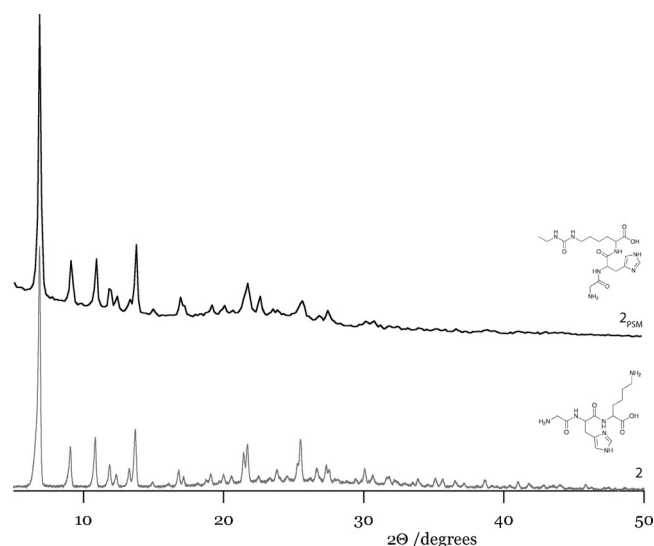


**Figure 5.** Structural integrity of Cu(GHK) modified post-synthetically. Comparison of the PXRD patterns for the as-made material (**2**) and after reaction with ethyl isocyanate (**2**<sub>PSM</sub>), confirming that the urea derivatization occurs without significant loss of crystallinity.

than those enabled by the use of shorter dipeptides. The structural stability of these materials remains limited by the rich conformational flexibility of the connectors as they undergo structural collapse when desolvated. However, they exhibit sponge-like amorphous-to-crystalline transformation when exposed to water and recover the open porous architecture. Our sorption studies indicate that this process does not involve recrystallization of the solids but is induced by the interaction of the guest molecules with the host via H-bond interactions with the FOS decorating the surface of the pores. This guest sorption-driven restructuring is accessible to flexible or soft frameworks.<sup>[27b,32]</sup>

Finally, we have made use of the aliphatic amine side-chain belonging to the lysine residue in **2** to demonstrate that the PSM protocols generally used for more rigid “classical” MOFs can be also exploited to post-synthetically modify these biomimetic materials for the first time. Hence, reaction with ethyl isocyanate at room temperature permits introducing urea functionalities in the framework with yields close to 80% and without significant decrease of crystallinity. On the basis of the catalytic activity of urea groups as hydrogen bond donors in aldol condensation reactions, this modification opens the door to studies on the potential application of these materials as individual catalysts (100% urea sites) or in cooperative catalysis by dual nucleophilic–electrophilic activation when both, unmodified amine and PSM-introduced urea groups, are present in the framework.<sup>[33]</sup> The retention of the open-framework architecture in the presence of solvents is consistent with the recovery of crystallinity upon water loading and permits liquid-phase processes such as this post-synthetic modification.

## Experimental Section

### Materials and methods

All reagents and solvents used were of commercially available grade and were used without any additional purification. The tripeptides H-Gly-L-His-Gly-OH and H-Gly-L-His-L-Lys-OH were acquired from Bachem® (<http://www.bachem.com>).

### Synthetic procedures

**[Cu(Gly-L-His-Gly)] (1; Gly-L-His-Gly = C<sub>12</sub>H<sub>16</sub>N<sub>6</sub>O<sub>5</sub><sup>2-</sup>):** This was prepared by dissolving 24.2 mg of the peptide (90 μmol) in 300 μL of an aqueous solution of Cu(OAc)<sub>2</sub>·2H<sub>2</sub>O 0.3 M (90 μmol) in a 4 mL glass vial. This synthetic procedure is based on previous studies describing the complexation of Cu<sup>II</sup> ions by glycylhistidylglycine in water.<sup>[34]</sup> The resulting blue mixture was mechanically stirred and, 1.26 mL of absolute ethanol and 200 μL of water, were sequentially added. The stirring was then stopped and the mixture left to stand at room temperature. This favoured the formation of blue coloured prismatic crystals, overnight. The crystalline product was then filtered from the reaction mixture, thoroughly washed with ethanol and stored in the fridge (75% yield). Elemental analysis calcd for [Cu(C<sub>12</sub>H<sub>16</sub>N<sub>6</sub>O<sub>5</sub>)·(H<sub>2</sub>O)<sub>6</sub>] (M<sub>w</sub> = 495.93): C 29.06, N 16.95, H 5.69; found: C 28.85, N 16.85, H 5.51. Elemental analysis calcd for the desolvated material (M<sub>w</sub> = 387.84): C 37.16, N 21.67, H 4.16; found: C 36.45, N 21.01, H 3.90.

**[Cu(Gly-L-His-L-Lys)] (2; Gly-L-His-L-Lys = C<sub>14</sub>H<sub>22</sub>N<sub>6</sub>O<sub>4</sub><sup>2-</sup>):** This was prepared by following a previously described methodology with minor modifications,<sup>[35]</sup> by dissolving 90 mg of the tripeptide (260 μmol) in 900 μL of an aqueous solution of copper(II) acetate 0.3 M (260 μmol) in a 12 mL glass vial. This change of colour is readily observed after the dissolution of the peptide. Next, 3.8 mL of absolute ethanol was added and the blue mixture was mechanically stirred for 5 min. This was followed by the addition of 1.2 mL of EtOH under static conditions, leading to the formation of a cloudy interphase. The vial was closed and left to stand at room temperature for 24 h. Finally, 3 mL of EtOH were added to the mixture. Although the formation of prismatic blue crystals in the bottom of the vial was detected after 24 h, the mixture was left to stand up to 48 h to maximise the yield of the reaction. Crystals were then filtered, thoroughly washed with ethanol and stored in the fridge (65% yield). Elemental analysis calcd for [Cu(C<sub>14</sub>H<sub>22</sub>N<sub>6</sub>O<sub>4</sub>)·(H<sub>2</sub>O)<sub>5</sub>] (M<sub>w</sub> = 491.98): C 34.18, N 17.08, H 6.56; found: C 33.68, N 16.58, H 6.40. Elemental analysis calcd for the desolvated material (M<sub>w</sub> = 401.91): C 41.84, N 20.91, H 5.52; found: C 41.55, N 20.66, H 5.66.

**Post-synthetic modification of 2:** A general protocol previously described for the reaction of metal-organic frameworks with isocyanates was followed.<sup>[31]</sup> Accordingly, 50 mg of as-made 2 was solvent-exchanged in 4 mL of chloroform during 3 days. Next, the crystals were filtered and suspended in 2 mL of CHCl<sub>3</sub> containing 8 equivalents of ethyl isocyanate (80 μL; 1 mmol). The reaction was left to progress at room temperature for 3 days. The crystals were then filtered, thoroughly washed with CHCl<sub>3</sub> to remove the excess of non-reacted isocyanate, and stored at 4 °C.

### Physical characterization

**Elemental analysis:** Carbon, nitrogen and hydrogen contents were determined by microanalytical procedures using a Thermo EA1112 Flash CHNS-O analyser.

**FT-IR spectroscopy:** Infrared spectra were collected from ground crystals in the 4000–400 cm<sup>-1</sup> range by using a PerkinElmer instrument Spectrum 100.

**Thermogravimetric analysis:** This was carried out with a SEIKO S-II instrument in the 25–450 °C temperature range under a 5 °C min<sup>-1</sup> scan rate and an air flow of 50 mL min<sup>-1</sup>.

**X-ray single-crystal data collection:** All single crystal data collections were undertaken using a Rigaku AFC12K goniometer with Mo<sub>Kα</sub> radiation from a Rigaku 007-HF Molybdenum rotating anode microfocus X-ray source and collected using Saturn 724 + CCD detector. Environmental control was achieved using a nitrogen stream from an Oxford Cryosystem 700 + Cryostream.<sup>[36]</sup> Data collections on compound 1, 2 were undertaken at 1° scan width in ω. A data collection of 1 × 170° and 2 × 125° ω-scans at 0, 120, 240°, respectively, with settings in φ and common setting of -68° in κ were employed for 1 whereas for 2 one of 3 × 125° ω-scans at 0, 120, 240° settings in φ and common setting of -68° in κ followed by a single 125° scan at κ = -30° and φ = 90° and final low angle 180° ω-scan at κ = φ = 0° were employed.

**X-ray powder diffraction:** XRPD patterns were collected in transmission geometry at 298 K by using a STOE Stadi-P diffractometer with Cu<sub>Kα</sub> radiation (λ = 1.54184 Å). Samples were ground and transferred to a 0.5 mm internal diameter glass capillary. Typically, profiles were collected as step scans over a 1.5 h period in the 5° < 2θ < 50° range with a step size of 0.25°.

**Gas sorption measurements:** The isotherms with CO<sub>2</sub> and H<sub>2</sub>O vapour were measured by using an intelligent gravimetric analyser (IGA) from Hidden Isochema Ltd. The samples were activated at 80 °C, overnight, before data collection. Isotherms for CO<sub>2</sub> were measured at 195 and 298 K at 1 and 10 bar, respectively. Water isotherms were collected between 20 and 38 °C up to the maximum pressure below the saturation vapour pressure of water at these temperatures. A "time-out" of 12 h was used for all measurements due to the slow equilibrium, this being the maximum time allowed for the determination of a single isotherm point.

**Scanning electron microscopy (SEM):** Images were collected on Hitachi S-4800 field-emission scanning electron microscope with energy dispersive X-ray (EDX) detector.

**NMR spectroscopy:** The <sup>1</sup>H NMR spectra were run on a Bruker AVANCE-400 MHz NMR spectrometer. In a typical experiment, 2 mg of 2<sub>PSM</sub> were readily dissolved in 1 mL of D<sub>2</sub>O followed by addition of Na<sub>2</sub>S(s) and mechanical stirring. This results in the precipitation of CuS as finely divided black solid, which was then removed from the solution by filtration. Table S2 in the Supporting Information summarizes the assignment of the obtained NMR spectra.

### Acknowledgements

Financial support from EPSRC under EP/H000925 is acknowledged. C.M.G. thanks the EU for a Marie Curie Fellowship (IEF-253369) and the Spanish MINECO for a Ramón y Cajal Fellowship (RYC-2012-10894).

**Keywords:** metal-organic frameworks • nanoporous materials • peptides • postsynthetic modifications • water adsorption

[1] See special issues on metal-organic frameworks and references therein: a) *Chem. Rev.* 2012; *Chem. Soc. Rev.* 2014; b) S. Kitagawa, R. Kitaura, S.-I.

- Noro, *Angew. Chem. Int. Ed.* **2004**, *43*, 2334–2375; *Angew. Chem.* **2004**, *116*, 2388–2430.
- [2] a) M. P. Suh, H. J. Park, T. K. Prasad, D.-W. Lim, *Chem. Rev.* **2012**, *112*, 782–835; b) K. Sumida, D. L. Rogow, J. A. Mason, T. M. McDonald, E. D. Bloch, Z. R. Herm, T.-H. Bae, J. R. Long, *Chem. Rev.* **2012**, *112*, 724–781; c) H. Chae, D. Siberio-Perez, J. Kim, Y. Go, M. Eddaoudi, A. Matzger, M. O’Keeffe, O. M. Yaghi, *Nature* **2004**, *427*, 523–527.
- [3] a) E. Bloch, W. L. Queen, R. Krishna, J. M. Zadrozny, C. M. Brown, J. R. Long, *Science* **2012**, *335*, 1606–1610; b) J. R. Li, J. Sculley, H. C. Zhou, *Chem. Soc. Rev.* **2012**, *112*, 869–932.
- [4] a) L. H. Wee, L. Alaerts, J. A. Martens, D. De Vos, *Metal–Organic Frameworks as Catalysts for Organic Reactions in Metal–Organic Frameworks: Applications from Catalysis to Gas Storage* (Ed.: D. Farrusseng), Wiley-VCH, Weinheim, **2011**, p. 191; b) A. Corma, H. García, F. Llabrés i Xamena, *Chem. Rev.* **2010**, *110*, 4606–4655; c) T. Zhang, W. Lin, *Chem. Soc. Rev.* **2014**, *43*, 5982–5993.
- [5] a) L. E. Kreno, K. Leong, O. K. Farha, M. Allendorf, R. P. Van Duyne, J. T. Hupp, *Chem. Soc. Rev.* **2012**, *112*, 1105–1125; b) B. Chen, L. Wang, Y. Xiao, F. R. Fronczek, M. Xue, Y. Cui, G. Qian, *Angew. Chem. Int. Ed.* **2009**, *48*, 500–503; *Angew. Chem.* **2009**, *121*, 508–511.
- [6] a) S. Horike, D. Umeyama, S. Kitagawa, *Acc. Chem. Res.* **2013**, *46*, 2376–2384; b) M. Yoon, K. Suh, S. Natarajan, K. Kim, *Angew. Chem. Int. Ed.* **2013**, *52*, 2688–2700; *Angew. Chem.* **2013**, *125*, 2752–2764.
- [7] a) Y. Liu, W. Xuan, Y. Cui, *Adv. Mater.* **2010**, *22*, 4112–4135; b) J. Seo, D. Whang, H. Lee, S. Im Jun, J. Oh, Y. Jeon, K. Kim, *Nature* **2000**, *404*, 982–986.
- [8] a) S. Hasegawa, S. Horike, R. Matsuda, S. Furukawa, K. Mochizuki, Y. Kinoshita, S. Kitagawa, *J. Am. Chem. Soc.* **2007**, *129*, 2607–2614; b) R. Kitaura, K. Fujimoto, S. Noro, M. Kondo, S. Kitagawa, *Angew. Chem. Int. Ed.* **2002**, *41*, 133–135; *Angew. Chem.* **2002**, *114*, 141–143.
- [9] a) Y.-X. Tan, Y.-P. He, J. Zhang, *Inorg. Chem.* **2012**, *51*, 11527–11531; b) R. Vaidhyanathan, D. Bradshaw, J.-N. Rebilly, J. P. Barrio, J. A. Gould, N. G. Berry, M. J. Rosseinsky, *Angew. Chem. Int. Ed.* **2006**, *45*, 6495–6499; *Angew. Chem.* **2006**, *118*, 6645–6649.
- [10] a) J. An, S. J. Geib, N. L. Rosi, *J. Am. Chem. Soc.* **2009**, *131*, 8376–8377; b) J. An, O. K. Farha, J. T. Hupp, E. Pohl, J. I. Yeh, N. L. Rosi, *Nat. Commun.* **2012**, *3*, 604; c) K. C. Stylianou, J. E. Warren, S. Y. Chong, J. Rabone, J. Bacsá, D. Bradshaw, M. J. Rosseinsky, *Chem. Commun.* **2011**, *47*, 3389–3391.
- [11] a) I. Imaz, M. Rubio-Martínez, J. An, I. Solé-Font, N. L. Rosi, D. Maspoch, *Chem. Commun.* **2011**, *47*, 7287–7302; b) V. Lillo, J. R. Galán-Mascarós, *Dalton Trans.* **2014**, *43*, 9821–9833.
- [12] A. P. Katsoulidis, K. Park, D. Antypov, C. Martí-Gastaldo, G. J. Miller, J. E. Warren, C. M. Robertson, F. Blanc, G. R. Darling, N. G. Berry, J. A. Purton, D. J. Adams, M. J. Rosseinsky, *Angew. Chem. Int. Ed.* **2014**, *53*, 193–198; M. J. Rosseinsky, *Angew. Chem. Int. Ed.* **2014**, *53*, 193–198; *Angew. Chem.* **2014**, *126*, 197–202.
- [13] J. Rabone, Y. F. Yue, S. Chong, K. C. Stylianou, J. Bacsá, D. Bradshaw, G. Darling, N. G. Berry, Y. Khimiyak, A. Ganin, P. Wiper, J. B. Claridge, M. J. Rosseinsky, *Science* **2010**, *329*, 1053–1057.
- [14] C. Martí-Gastaldo, D. Antypov, J. E. Warren, M. E. Briggs, P. A. Chater, P. V. Wiper, G. Miller, Y. Z. Khimiyak, G. R. Darling, N. G. Berry, M. J. Rosseinsky, *Nat. Chem.* **2014**, *6*, 343–351.
- [15] C. Martí-Gastaldo, J. E. Warren, K. C. Stylianou, N. L. O. Flack, M. J. Rosseinsky, *Angew. Chem. Int. Ed.* **2012**, *51*, 11044–11048; *Angew. Chem.* **2012**, *124*, 11206–11210.
- [16] P. de Meester, D. J. Hodgson, *Acta Crystallogr. Sect. A* **1977**, *33*, 3505–3510.
- [17] C. Hureau, H. Eury, R. Guillot, C. Bijani, S. Sayen, P.-L. Solari, E. Guillon, P. Faller, P. Dorlet, *Chem. Eur. J.* **2011**, *17*, 10151–10160.
- [18] a) H. D. Flack, *Acta Crystallogr. Sect. A* **1983**, *39*, 876–881; b) R. W. W. Hoof, L. H. Straver, A. L. Spek, *J. Appl. Crystallogr.* **2008**, *41*, 96–103.
- [19] H. C. Freeman, *Crystal Structure of Metal–Peptide Complexes, in Advances in Protein Chemistry, Vol. 22* (Ed.: C. B. Afinsen), Academic Press, **1967**, p. 258.
- [20] a) G. B. McGaughey, M. Gagne, A. K. Rappe, *J. Biol. Chem.* **1998**, *273*, 15458–15463; b) R. J. Sundberg, R. B. Martin, *Chem. Rev.* **1974**, *74*, 471–517.
- [21] H. C. Freeman, J. Guss, M. J. Healy, R.-P. Martin, C. E. Nockolds, B. Sarkar, *J. Chem. Soc. D* **1969**, 225–226.
- [22] Parameters calculated with CALCVOID, CALCSOLV as implemented in Olex2: O. V. Dolomanov, L. J. Bourhis, R. J. Gildea, J. A. K. Howard, H. Puschmann, *J. Appl. Crystallogr.* **2009**, *42*, 339–341.
- [23] Metrics of the porosity were calculated with Zeo++: T. F. Willems, C. H. Rycroft, M. Kazi, J. C. Meza, M. Haranczyk, *Microporous Mesoporous Mater.* **2012**, *149*, 134–141.
- [24] E. Davie, S. Mennen, Y. Xu, S. Miller, *Chem. Rev.* **2007**, *107*, 5759–5812.
- [25] L. Carlucci, G. Ciani, M. Moret, D. M. Proserpio, S. Rizzato, *Angew. Chem. Int. Ed.* **2000**, *39*, 1506–1510; *Angew. Chem.* **2000**, *112*, 1566–1570.
- [26] D. Maspoch, D. Ruiz-Molina, K. Wurst, N. Domingo, M. Cavallini, F. Biscarini, J. Tejada, C. Rovira, J. Veciana, *Nat. Mater.* **2003**, *2*, 190–195.
- [27] a) S. Horike, S. Shimomura, S. Kitagawa, *Nat. Chem.* **2009**, *1*, 695–704; b) S. Kitagawa, K. Uemura, *Chem. Soc. Rev.* **2005**, *34*, 109–119.
- [28] J. Ferrando-Soria, R. Ruiz García, J. Cano, S.-E. Stiriba, J. Vallejo, I. Castro, M. Julve, F. Lloret, P. Amorós, J. Pasán, C. Ruiz-Pérez, Y. Journaux, E. Pardo, *Chem. Eur. J.* **2012**, *18*, 1608–1617.
- [29] *CRC Handbook of Chemistry and Physics*, 74th ed., The Chemical Rubber Co., Boca Raton, **1993**.
- [30] a) S. M. Cohen, *Chem. Soc. Rev.* **2012**, *112*, 970–1000; b) M. J. Ingleson, J. P. Barrio, J.-B. Guilbaud, Y. Z. Khimiyak, M. J. Rosseinsky, *Chem. Commun.* **2008**, 2680–2682.
- [31] E. Dugan, Z. Wang, M. Okamura, A. Medina, S. M. Cohen, *Chem. Commun.* **2008**, 3366–3368.
- [32] A. Schneemann, V. Bon, I. Schwedler, I. Senkovska, S. Kaskel, R. A. Fischer, *Chem. Soc. Rev.* **2014**, *43*, 6062–6096.
- [33] E. L. Margelefsky, R. K. Zeidan, M. E. Davis, *Chem. Soc. Rev.* **2008**, *37*, 1118–1126.
- [34] a) R. Österberg, B. Sjöberg, R. Söderquist, *J. Chem. Soc. Chem. Commun.* **1972**, 983–985; b) R. Österberg, B. Sjöberg, *Acta Chem. Scand.* **1972**, *26*, 4184–4185.
- [35] C. Perkins, N. Rose, E. Weinstein Ronald, *Inorg. Chim. Acta* **1984**, *82*, 93–99.
- [36] J. Cosier, A. M. Glazer, *J. Appl. Crystallogr.* **1986**, *19*, 105–107.

Received: May 29, 2015

Revised: August 18, 2015

Published online on September 25, 2015